Methods in Oceanography 12 (2015) 18–35

Contents lists available at ScienceDirect

Methods in Oceanography

journal homepage: www.elsevier.com/locate/mio

Full length article

Assessment of trawlable and untrawlable seafloor using multibeam-derived metrics

Jodi L. Pirtle [a,*,1], Thomas C. Weber [a], Christopher D. Wilson [b], Christopher N. Rooper [b]

[a] University of New Hampshire, Center for Coastal and Ocean Mapping, 24 Colovos Road, Durham, NH, 03824, USA

[b] National Oceanic and Atmospheric Administration, National Marine Fisheries Service, Alaska Fisheries Science Center, 7600 Sand Point Way NE, Seattle, WA, 98115, USA

ARTICLE INFO

Article history:
Received 28 January 2015
Received in revised form
22 May 2015
Accepted 5 June 2015
Available online 1 July 2015

Keywords:
Acoustic backscatter
Multibeam echosounder
Terrain analysis
Seafloor characterization
Bottom-trawl survey
Groundfish habitat
Trawlable
Untrawlable
Gulf of Alaska

ABSTRACT

Groundfish that associate with rugged seafloor types are difficult to assess with bottom-trawl sampling gear. Simrad ME70 multibeam echosounder (MBES) data and video imagery were collected to characterize trawlable and untrawlable areas, and to ultimately improve efforts to determine habitat-specific groundfish biomass. The data were collected during two acoustic-trawl surveys of the Gulf of Alaska (GOA) during 2011 and 2012 by NOAA Alaska Fisheries Science Center (AFSC) researchers. MBES data were collected continuously along the trackline, which included parallel transects (1–20 nmi spacing) and fine-scale survey locations in 2011. Video data were collected at camera stations using a deployed camera system. Multibeam-derived seafloor metrics were overlaid with the locations of previously conducted AFSC bottom-trawl (BT) survey hauls and 2011 camera stations. Generalized linear models were used to identify the best combination of multibeam metrics to discriminate between trawlable and untrawlable seafloor for the region of overlap between the camera stations or haul paths and the MBES data. The two best models were developed using data collected at camera stations with either oblique incidence backscatter strength (S_b) or mosaic S_b in combination with bathymetric posi-

* Corresponding author. Tel.: +1 907 789 6603; fax: +1 907 789 6094.
E-mail address: jodi.pirtle@noaa.gov (J.L. Pirtle).

[1] Present address: National Academy of Sciences, National Research Council, Visiting Scientist at National Oceanic and Atmospheric Administration, National Marine Fisheries Service, Alaska Fisheries Science Center, 17109 Point Lena Loop Road, Juneau, AK, 99801, USA.

http://dx.doi.org/10.1016/j.mio.2015.06.001

tion index and seafloor ruggedness; these described over 54% of the variation between trawlable and untrawlable seafloor types. A map of predicted seafloor trawlability produced from the model using mosaic S_b and benthic-terrain metrics demonstrated that 58% of the area mapped (5987 km^2) had $\geq$50% probability of being trawlable and 42% of being untrawlable. The model correctly predicted 69% of trawlable and untrawlable haul locations. Successful hauls occurred in areas with 62% probability of being trawlable and gear damage occurred in areas with a 38% probability of being trawlable. This model and map produced from multibeam-derived seafloor metrics may be used to refine seafloor interpretation for the AFSC BT surveys and to advance efforts to develop habitat-specific biomass estimates for GOA groundfish populations.

1. Introduction

Multi-species bottom-trawl surveys are a common fishery-independent assessment method to obtain biomass estimates for demersal fish populations. Inherent in trawl survey biomass estimates is the issue of catchability, which is influenced by the relative proportion of trawlable and untrawlable ground in a survey area, or the area accessible by the survey (Cordue, 2007). Management areas like the Gulf of Alaska and US West Coast have a mix of trawlable and untrawlable seafloor types (Zimmermann, 2003; Von Szalay et al., 2010). Certain groundfish species, such as rockfishes (*Sebastes* spp.) have mixed distribution in trawlable and untrawlable habitat or prefer rugged habitat inaccessible to bottom-trawl gear (Stein et al., 1992; Clausen and Heifetz, 2002; Jagielo et al., 2003; Rooper et al., 2007). Consequently, the proportion of the population in untrawlable habitat is undersampled or not sampled at all, and the sampled population is assumed to be representative of the entire population for the purpose of the stock assessment. Disproportionate survey access to all areas occupied by the harvested population can introduce non-random error to biomass estimates from trawl survey time-series (Cordue, 2007). Thus, more accurate accounting of the extent of trawlable and untrawlable survey area is needed as a first step toward assessing and correcting this potential bias.

National Oceanic and Atmospheric Administration (NOAA) Alaska Fisheries Science Center (AFSC) Resource Assessment and Conservation Engineering (RACE) Division researchers conduct a biennial area-wide bottom-trawl survey (BT survey) for groundfish in the Gulf of Alaska (GOA), from the Islands of Four Mountains (169°59′0″W 52°43′11″N) in the Aleutian Islands to Dixon Entrance (133°13′53″W 54°30′38″N) (Von Szalay et al., 2010). The RACE BT survey is conducted aboard chartered commercial fishing vessels. Stations in 59 survey strata are allocated from a sampling grid in a stratified-random design. A survey vessel skipper searches to locate trawlable ground within a station grid cell for a minimum of two hours, or abandons that cell and searches within another until trawlable ground is located. The sampling grid is populated with the locations of known trawlable and untrawlable features. However, knowledge of seafloor trawlability is not comprehensive across a survey grid cell and is qualitative at best. Untrawlable seafloor is often encountered in areas thought to be trawlable, which can result in considerable gear damage and loss of the sample and survey time. Given the difficulties in selecting trawlable seafloor, we know that there are similar difficulties associated with identifying untrawlable seafloor. A better estimate of the areal extent of trawlable and untrawlable ground in the GOA will improve biomass estimates for groundfish, increase survey efficiency, and reduce damage to gear and benthic habitat. In this study, we test metrics derived from multibeam echo sounder (MBES) data for their ability to discriminate between trawlable and untrawlable seafloor types in the RACE BT survey area.

MBES surveys can acquire high-resolution bathymetry and backscatter data concurrently to produce detailed images of the seafloor. Several quantitative metrics can be derived from MBES data to distinguish seafloor features of varied morphology (e.g., Wilson et al., 2007). When combined with groundtruth data of similar spatial scale, it is possible to model and map seafloor types and landscape features that influence marine species distribution (Dolan et al., 2008; Buhl-Mortensen et al., 2009; Reynolds et al., 2012), including habitat for harvested species (Shotwell et al., 2008; Todd and Kostylev, 2011). Metrics extracted from MBES data that may be useful predictors to discriminate between areas of trawlable and untrawlable seafloor include those derived from angle-dependent backscatter strength, backscatter mosaics, and bathymetry.

Seafloor backscatter strength (S_b) is dependent on the incident angle of sound with the seafloor. For example, the predicted S_b (decibels; dB) of a cobble seafloor is quite similar to fine sand and silt when examined at angles near normal incidence (0°). In contrast, the S_b of cobble is predicted to be well separated from sediments of finer grain sizes at oblique incidence angles between 30° and 50° (APL, 1994; Weber et al., 2013). Studies have used multibeam-derived angle-dependent S_b metrics to describe the nature of seafloor sediments (Fonseca and Mayer, 2007; Fonseca et al., 2009), terrain features (Weber et al., 2013), and benthic habitat (Hasan et al., 2012). The ability of angle-dependent S_b metrics to discriminate between trawlable and untrawlable seafloor has been tested for a small region containing a subset of the seafloor types present in the GOA (Weber et al., 2013).

Mosaics are a commonly used form of backscatter data. Mosaics are generated by normalizing S_b values across the multibeam swath to the range of observed values at oblique incidence angles (e.g., Rzhanov et al., 2012). One caveat to working with mosaics is the assumption that normal incidence backscatter strength has the same discriminatory power as backscatter strength from oblique incidence angles. Some angular resolution of the S_b data is also lost when mosaics are produced. However, backscatter mosaics have the potential to simplify interpretation of seafloor properties, as opposed to retaining and analyzing the full angle-dependent S_b. Greater spatial resolution is also available from backscatter mosaics, as opposed to angle-dependent S_b metrics that apply to discrete sections of the multibeam swath.

Several benthic terrain metrics can be derived from high-resolution multibeam bathymetry data that describe attributes of seafloor morphology. Seafloor slope, curvature, and bathymetric position index are measures of terrain variability. Seafloor slope is the rate of change in bathymetry over a defined area (Horn, 1981). Seafloor curvature highlights concave and convex slopes and defines sloping terrain along features (Evans, 1980; Schmidt et al., 2003). Bathymetric position index (BPI) is the equivalent of topographic position index, which describes the elevation of one location relative to the mean of neighboring locations (Guisan et al., 1999; Weiss, 2001). BPI will emphasize features that are shallower or deeper than the surrounding area, such as ridges and valleys. Seafloor ruggedness is a measure of terrain complexity that highlights the presence of rough and bathymetrically uneven terrain (Sappington et al., 2007). Examining these terrain metrics at fine and broad spatial scales may be meaningful to determine the relative influence of features of different scale to distinguish between trawlable and untrawlable seafloor types.

We derived several metrics that describe the seafloor in the GOA from data collected opportunistically with a Simrad ME70 MBES, during ongoing fishery resource surveys. The ME70 is a calibrated MBES designed to collect quantitative acoustic data on targets throughout the water column (Trenkel et al., 2008; Cutter et al., 2010). Bathymetry and backscatter data are acquired concurrently when the ME70 is operated in the standard fishery mode. User configuration is possible and bottom detections can be extracted from the data with customized software designed to characterize the seafloor in the area of study (Weber et al., 2013).

In this work, we demonstrate the value of multibeam metrics as predictor variables to discriminate between trawlable and untrawlable seafloor types in the GOA, extending the preliminary study by Weber et al. (2013). Our objectives were to (1) determine whether or not trawlable and untrawlable ground can be distinguished using a variety of multibeam-derived backscatter and bathymetry metrics; (2) identify which multibeam metrics, singularly or in combination, are most useful to discriminate between trawlable and untrawlable locations; and (3) generate probability maps of predicted seafloor trawlability within the GOA.

2. Methods

2.1. Multibeam survey

NOAA AFSC RACE researchers conduct acoustic-trawl surveys (AT surveys) with the NOAA ship *Oscar Dyson* to assess semi-demersal walleye pollock (*Gadus chalcogrammus*) biomass and distribution during summer and winter in the GOA (Jones and Guttormsen, 2012; Jones et al., 2015). ME70 data were collected during the summer 2011 GOA-wide biennial AT survey from 14 June to 12 August from the Islands of Four Mountains in the Aleutian Islands (169°59′0″W 52°43′11″N) to the eastern side of Kodiak Island (151°5′25″W 57°20′46″N). Additional ME70 data were collected during the smaller-scale winter 2012 AT survey during 13–22 February and 17–27 March between Sanak Island (163°14′42″W 54°48′37″N) and the eastern side of Kodiak Island. Survey activities for the pollock assessment were generally conducted during daylight hours in the summer and both day and night during the winter pre-spawning pollock AT surveys. Nominal underway free-running (versus trawling) vessel speed was 5.5–6 m s^{-1} (10.7–11.7 kt), but varied depending on weather and sea state.

The ME70 was operated in fishery mode, using a custom configuration of 31-beams at frequencies from 73–117 kHz, with beam opening angles from 2.8°–11.0°, steered to 0° in the alongship direction and −66° to +66° in the athwartship direction, with the lowest frequencies steered to the highest beam angles, and a pulse duration of 1.5 m s^{-1} (*sensu* Weber et al., 2013). The ME70 was calibrated in Three Saints Bay, Kodiak Island (153°30′54″W 57°10′30″N), prior to the start of the summer 2011 survey, using the standard sphere calibration method (Foote et al., 1987).

ME70 data were collected during the surveys along parallel transects spaced 2–20 nmi apart over 20–500 m bottom depths. Fine-scale multibeam surveys with 100% bottom coverage were conducted during evening hours of the summer 2011 survey to target both trawlable and untrawlable seafloor types. An Applanix POS/MV V4 system output dynamic motion and position data directly to the ME70 to compensate the beam directions for pitch and roll of the ship and to georeference the multibeam data. A C-Nav MBX-4 system applied differential correction data to the POS/MV to improve position accuracy. Expendable bathythermograph (XBT) profiles were conducted approximately every 3–6 h during the survey and conductivity temperature and depth (CTD) sensor profiles were conducted nightly at fine-scale survey locations to measure sound speed through the water column and correct for the effect of sound refraction. Conductivity and temperature were also continuously measured near the transducer by the ME70 system.

2.2. Camera stations

Video imagery was collected at camera stations to characterize the seafloor as trawlable or untrawlable for comparison with the ME70 data. Camera stations were sampled during evening hours of the summer 2011 survey within the fine-scale multibeam survey areas. Camera stations were located in a pattern that sampled a central location and then targeted the remaining fine-scale survey area equally. One camera deployment was conducted at each camera station. At least one and as many as five camera stations were sampled during each fine-scale survey.

Video imagery was collected at camera stations using one of two camera systems, including a single camera (DC) and stereo camera (SDC) system. The DC was fitted with one digital video recorder and two lights placed above the camera housing for illumination. The SDC had two-Sony TRD-900 progressive scan camcorders with 1280 × 720 pixel resolution (Sony Corp., Tokyo, Japan) and two lights placed above the camera housings (Williams et al., 2010). Both systems were mounted in aluminum cages.

Each DC deployment via standard shipboard winch included 5 min of total bottom time providing a visual assessment of the seafloor. Each SDC deployment included 30 min total bottom time. Unlike the DC, the SDC used a real-time video feed and a dedicated winch which allowed vertical maneuverability in the water column and over the benthic terrain. This system was optimal for greater spatial coverage and was used when more ship time was available.

Seafloor substrate was classified from video, using a two-code system with the following categories: rock with vertical relief (R), flat bedrock (F), boulder (B; >25.5 cm), cobble (C; 6.5–25.5 cm), pebble (P; 2–6.5 cm), gravel (G; 2–4 mm), sand (S; grains distinguishable), and mud

(M) (Wentworth, 1922; Stein et al., 1992). Grain size was estimated from a tethered weight (28 cm diameter) in the field of view (DC), or directly from the horizontal field of view (2.4 m; SDC). The first code with this system represented 50%–80% of the substrate composition, and the second code represented 20%–50% (e.g., MB is at least 50% mud and at least 20% boulder, and BB is $\geq$80% boulder). A new code was assigned when a change in substrate was encountered for an area lasting greater than 10 s of video duration.

The seafloor substrate and overall benthic terrain at camera stations was further classified as trawlable or untrawlable. A standard Poly-Nor'eastern 4-seam bottom-trawl is used in the GOA BT survey (Stauffer, 2004). Untrawlable areas for this study were defined as any substrate containing boulders (>25.5 cm at the greatest dimension) reaching higher than 20 cm off bottom, or bedrock with vertical relief and–or ruggedness that would likely prevent the bottom-trawl from passing over it without damage from seafloor contact.

2.3. Haul locations

Historic BT survey haul locations were sampled with the ME70 whenever possible during the AT surveys. Because the bottom-trawl haul locations occurred in areas that were assumed to be trawlable by the BT survey, the haul locations represent only a subset of the seafloor types in the GOA. In contrast, the camera stations sampled during the multibeam survey captured a variety of trawlable and untrawlable seafloor types that were characterized from video. Due to this difference, the haul locations and camera stations were compared to the ME70 data as separate data sets.

Haul location samples were constrained to survey years 1996–2011, due to positional precision and reliable trawl gear damage reporting. Haul performance is characterized by RACE as successful, marginally-successful (hereafter marginal), or failed, based on the level of gear damage sustained from seafloor contact. Successful hauls do not sustain gear damage and provide an acceptable catch sample. Marginal hauls are those with some gear damage, but where the damage was judged to not affect the catch. Failed hauls have extensive gear damage, or the damage was located in an area of the net where the catch was judged to be affected. Bottom-trawl hauls used in our analysis incurred several types of failure resulting in gear-damage, including gear hang-ups (i.e., gear was snagged or entangled on the seafloor), having to haul-back early due to hangs, major hangs that stopped the forward progress of the vessel, and on two occasions the net was destroyed. Successful hauls were assumed to occur in areas of trawlable seafloor and failed hauls in areas of untrawlable seafloor. Marginal hauls were pooled with failed hauls for the analysis because all hauls with gear damage were assumed to occur in locations with untrawlable features.

2.4. Multibeam data

2.4.1. Multibeam data processing

The Simrad ME70 data collection and processing workflow for this study is shown in Fig. S1 (see Appendix A). Raw acoustic data files were generated by the ME70 workstation during data collection. Bathymetry and S_b data were extracted from the raw ME70 files using algorithms that perform bottom detections and apply uncertainty corrections (*sensu* Weber et al., 2013). The bottom detections were then used to calculate angle-dependent S_b metrics for data analysis, or written to Generic Sensor Format (GSF) files for further processing.

2.4.2. Angle-dependent S_b

Three different angle-dependent S_b metrics were derived from the seafloor backscatter strength. These were based on the predicted S_b at incidence angles (Jackson and Richardson, 2007). These metrics were normal-incidence S_b (0°–1°), oblique incidence S_b (30°–50°), and the slope of the angle-dependent backscatter within 10° of normal incidence (S_b-slope).

2.4.3. Backscatter mosaics and bathymetry grids

Bottom detections from the ME70 data were input as GSF files into the hydrographic data processing software CARIS HIPS (version 7.2, CARIS). Soundings were corrected for vessel offsets, sound

refraction, and tides, and merged to generate a 6 m^2 resolution surface, using the Combined Uncertainty and Bathymetric Estimator algorithms (CUBE). Cursory cleaning was conducted to remove obvious sounding errors affecting the surface. Processed GSF files were exported to Fledermaus Geocoder Tools (FMGT) and DMagic to generate backscatter mosaics (S_b, dB) and bathymetry grids (m-depth), each at 6 m^2 resolution (version 4.0, IVS).

2.4.4. Benthic terrain analysis

Benthic terrain metrics were derived from bathymetry grids (6 m^2) in ArcGIS (version 10.1, ESRI). Calculations for seafloor slope and curvature were performed using DEM Surface Tools (Jenness, 2013). Seafloor ruggedness and BPI were calculated using features of the Benthic Terrain Modeler (Wright et al., 2012). Seafloor slope, curvature, and ruggedness were calculated from a moving analysis window of a 3×3 array of grid cells, which uses the bathymetry of each cell and 8 surrounding neighbors. Ruggedness was also calculated using 11 and 21 cell arrays. These spatial scales were selected based on the scale of terrain features derived by these metrics that are likely encountered by a bottom-trawl haul path (16 m width). Slope was calculated along east–west and north–south gradients, using Horn's directional method (Horn, 1981). Two measures of curvature were calculated. Profile curvature is the curvature of the surface in the maximum direction of slope, and is useful to highlight concave and convex slopes. Plan curvature is the curvature perpendicular to the maximum direction of slope, and is useful to define sloping terrain along features (Evans, 1980; Schmidt et al., 2003). Seafloor ruggedness was calculated using a vector ruggedness measure (VRM) that quantifies the 3-dimensional dispersion of vectors orthogonal to the planar terrain surface and accounts for variability in both slope and aspect (Sappington et al., 2007). BPI compares the bathymetric position of a grid cell to the mean of neighboring cells in radial directions (Guisan et al., 1999; Weiss, 2001). BPI was calculated from neighborhoods with a radius of 20, 50, 100, and 200 cells.

2.5. Data analysis

2.5.1. Extract multibeam metrics

Two sets of sample locations were used for this analysis. These included the camera stations within the ME70 fine-scale survey areas and BT survey trawl haul locations. Multibeam-derived seafloor metrics were overlaid with the location of camera stations and haul path locations to extract metrics that could potentially discriminate between trawlable and untrawlable seafloor types and to generate models and probability maps of predicted seafloor trawlability. Multibeam metrics were extracted from an area within 20 m of the camera stations. Multibeam metrics were extracted at haul locations for the area of overlap between the ME70 swath and bottom-trawl path where the net was in contact with the seafloor, taking into account the distance of wire out, trawl warp length, trawl width (16 m), and the positional uncertainty of the survey vessel. A 28 m buffer around the haul paths was applied to additionally include one half of the trawl net width (8 m). Haul paths targeted during the multibeam survey were sampled with 100% coverage. Occasionally, only the edge or a section of a haul path was sampled because of the opportunistic nature of ME70 operations during the AT surveys. Multibeam survey coverage of individual haul path locations was determined based on the proportion of the haul path area sampled by the multibeam swath. Analysis was limited to haul locations where the region of overlap between the multibeam data and bottom-trawl haul path location was $>10\%$ of the haul path area.

The multibeam data extracted for analysis with the camera and haul data sets included angle-dependent S_b metrics, backscatter and bathymetry metrics as well as their associated mean and standard deviation (SD). These calculations were performed for S_b metrics (dB) by first converting those values to intensities. Metrics used in data analysis are listed in Table 1. To determine whether a multibeam-derived metric could discriminate between trawlable and untrawlable areas, the metric values of camera stations and haul locations that were characterized as trawlable or untrawlable were first compared using a 2-sample t-test ($\alpha = 0.05$).

Table 1
Seafloor metrics derived from data collected with the ME70 MBES during cruises in 2011 and 2012 aboard the NOAA ship *Oscar Dyson* in the Gulf of Alaska. Metrics derived from the angle-dependent seafloor backscatter strength (S_b) were normal-incidence seafloor S_b, oblique incidence S_b, and the slope of the angle-dependent backscatter within 10° of normal incidence (S_b-slope). The mean mosaic value (mosaic S_b) was derived from backscatter mosaics. Metrics derived from gridded bathymetry data were seafloor slope, plan curvature, profile curvature, ruggedness (VRM), and bathymetric position index (BPI).

Multibeam metric	Angle of incidence or scale
Angle-dependent S_b	Raw data resolution
Normal incidence S_b	0°–1°
Oblique incidence S_b	30°–50°
S_b-slope	0°–10°
Backscatter mosaic	6 m^2
Mosaic value	Swath normalized to values from 30°–50°
Bathymetry grid	6 m^2
Slope	3 × 3 cells
Profile curvature	3 × 3 cells
Plan curvature	3 × 3 cells
VRM	3 × 3, 11 × 11, 21 × 21 cells
BPI	20, 50, 100, 200 cell radius

2.5.2. Model seafloor trawlability

The ability of each multibeam-derived metric to discriminate between trawlable and untrawlable areas was tested with predictive models. Seafloor trawlability was modeled separately for camera stations and haul locations with logistic regression using a generalized linear model (GLM) $Y = \propto +\beta_1 X_1 + \beta_i X_i + E$ and the logit link function $p(Y) = \exp(Y)/(1 + \exp(Y))$ for binary response data (McCullagh and Nelder, 1983). GLM can accommodate data that are not normally distributed and the model results can be implemented as probability maps for prediction (Guisan et al., 1999; Duff, 2008). The response for these models was the trawlable or untrawlable characterization for each sample location. Predictor variables were the multibeam-derived seafloor metrics at the sample locations (Table 1). Multibeam metrics were standardized prior to analysis by subtracting the mean and dividing by the SD of the metric. Best-fitting models were determined in a forward step-wise fashion beginning with the camera stations.

Models with metrics as individual predictors were examined first. Common diagnostics for logistic regression were evaluated, including the proportion of deviance explained (D^2) and an analysis of deviance test. An analysis of deviance test is a likelihood ratio test for GLMs used to evaluate the performance of each model compared to a null model ($\alpha = 0.05$). The most discriminatory models were chosen based on the Akaike information criterion (AIC). Models with AIC values within 2 digits are not considered different with regard to the predicted response (Burnham and Anderson, 2002).

Models with more than one predictor were examined next, using combinations of the best individual predictor models. Multi-collinearity among multibeam metrics was examined prior to choosing metrics for models with more than one predictor, so that collinear metrics ($|r| > 0.7$) were not included in the same model (e.g., Dormann et al., 2013). Predictors were added one by one as long as the model fit improved. The best models with more than one predictor were evaluated and compared to the results of the single predictor models. All analysis was conducted in R (R Development Core Team, 2013).

2.5.3. Map seafloor trawlability

Predicted probability of seafloor trawlability for the GOA multibeam survey area was mapped using the model coefficients and multibeam metrics from the best model. A model probability threshold of 0.5 was used to discriminate between trawlable and untrawlable areas. The ability of the model to correctly predict the presence of trawlable and untrawlable seafloor features was evaluated for either camera stations or haul locations, depending on which data set was used with the MBES survey data to develop the best model. This cross-validation analysis was conducted in ArcGIS by extracting the

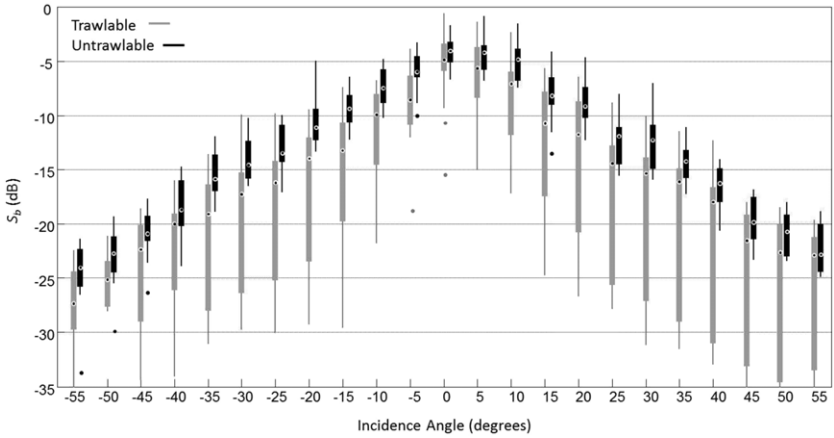

Fig. 1. Distribution of angle-dependent seafloor backscatter strength values (S_b; dB) for the range of incidence angles (−55°–+55°) sampled by the multibeam swath at camera stations classified as trawlable or untrawlable. Camera stations ($n = 47$) were sampled during the 2011 ME70 MBES survey aboard the NOAA ship *Oscar Dyson* in the GOA.

model values of predicted seafloor trawlability from the region of overlap with sample locations that were classified as trawlable or untrawlable.

3. Results

A total of 47 camera stations were sampled at fine-scale ME70 survey locations during the 2011 AT survey. Trawlable seafloor was identified at 27 camera stations and untrawlable seafloor at 20 stations (Table S1; see Appendix A).

Seafloor substrate at trawlable camera stations included poorly sorted, fine-grain sediments, which were difficult to distinguish from one another in the video data (e.g., mixed sand and mud with silt). Other substrate types at the trawlable camera stations were more readily discernible and included areas of fine-grain sediments with scattered gravel, pebbles, cobbles, and the occasional embedded small boulder, or continuous areas of gravel and pebbles with scattered cobbles of varied size. Untrawlable stations included areas of fine-grain sediment with boulders and rock outcrops, areas of continuous gravel, pebbles, and cobble with isolated boulders and rock, or areas of continuous boulder and rock.

The total area mapped with the ME70 during the AT surveys was 5987 km^2, which corresponded with the location of 450 historic bottom-trawl haul paths across the BT survey area. These included 373 successful hauls and 77 marginal and failed hauls. The range of spatial overlap between the multibeam data (swath) and individual haul locations was 10%–100% with mean overlap of 55% (±26% SD). Examining the distribution of seafloor scattering strength data at the range of angles across the multibeam swath demonstrated that areas of trawlable seafloor generally exhibited lower S_b values than areas with untrawlable seafloor. Areas of trawlable seafloor at camera stations generally had lower S_b values at all incidence angles than untrawlable seafloor (Fig. 1). The BT survey haul performance categories, successful, marginal, and failed, show separation in S_b values across incidence angles at haul locations, with successful haul locations having lower values overall (Fig. 2). Marginal and failed haul locations grouped together in the range of higher S_b values across the multibeam swath. Mean S_b values at marginal and failed haul locations were not significantly different.

3.1. Multibeam metrics and camera stations

Angle-dependent S_b metric values (Table 1) for camera stations classified as trawlable were significantly lower than those classified as untrawlable (Fig. 3). Similar results were obtained for values

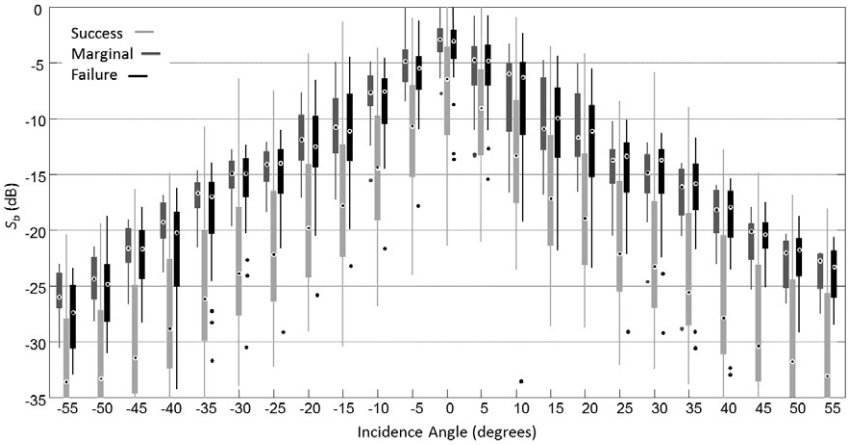

Fig. 2. Distribution of angle-dependent seafloor backscatter strength values (S_b; dB) for the range of incidence angles (−55°–+55°) sampled by the multibeam swath at haul locations where trawl performance was classified as successful, marginal, or failed. Haul locations sampled ($n = 450$) were conducted during the summer 1996–2011 RACE BT surveys.

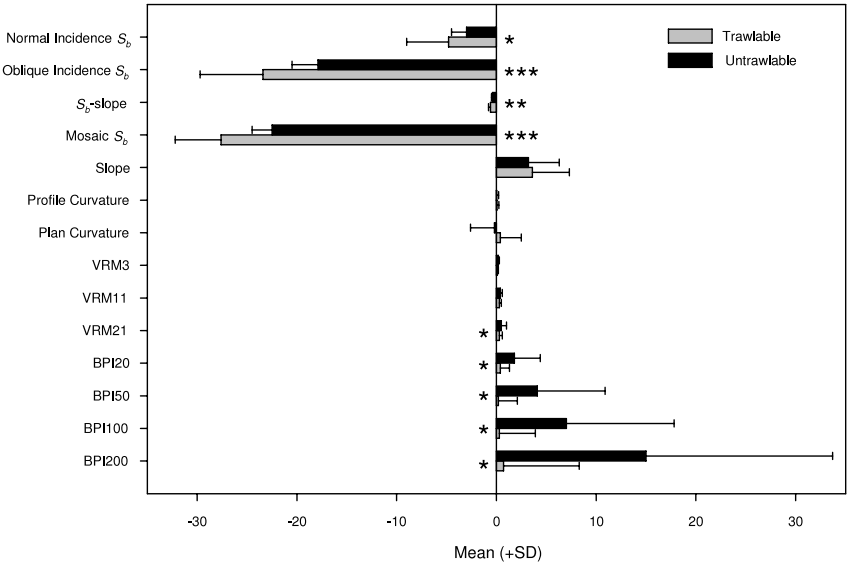

Fig. 3. Multibeam-derived seafloor metrics (mean, +SD) compared between trawlable and untrawlable camera stations (t-test, $\alpha = 0.05$). Metrics derived from the angle-dependent seafloor backscatter strength (S_b) are normal-incidence S_b, oblique incidence S_b, and S_b-slope. Mosaic S_b is derived from backscatter mosaics (6 m^2). Metrics derived from gridded bathymetry data (6 m^2) are seafloor slope, profile curvature, and plan curvature, calculated from 3 × 3 cell arrays. Seafloor ruggedness (VRM) is calculated from 3 × 3, 11 × 11, and 21 × 21 cells, and bathymetric position index (BPI) is calculated from 20, 50, 100, and 200 cell radius analysis windows. Significance levels are as follows: * ($p < 0.05$), ** ($p < 0.001$), *** ($p < 0.0001$).

derived from backscatter mosaics. Mosaic S_b values were significantly lower at trawlable camera stations.

Differences were detectable between trawlable and untrawlable camera stations for only some of the benthic terrain metrics derived from the bathymetry grids (Fig. 3). All BPI values were significantly less at trawlable camera stations. Measures of seafloor slope and curvature did not distinguish between trawlable and untrawlable stations. Differences were also not detectable between trawlable

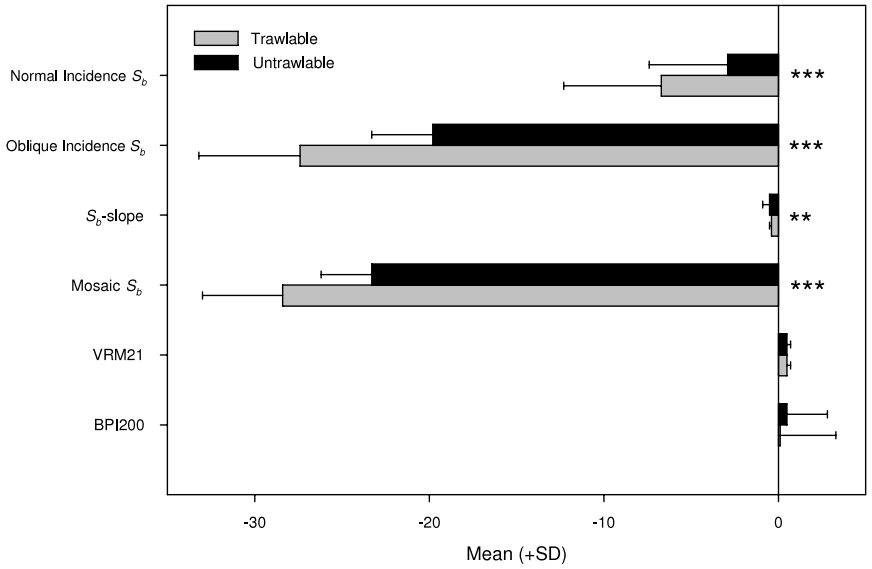

Fig. 4. Multibeam-derived seafloor metrics (mean, +SD) compared between trawlable and untrawlable historic bottom-trawl haul locations (t-test, $\alpha = 0.05$). Metrics derived from the angle-dependent seafloor backscatter strength (S_b) are normal-incidence S_b, oblique incidence S_b, and S_b-slope. Mosaic S_b is derived from backscatter mosaics (6 m^2). Metrics derived from gridded bathymetry data (6 m^2) are seafloor ruggedness (VRM) calculated from a 21 × 21 cell array, and bathymetric position index (BPI) calculated from an analysis window of 200 cell radius. Significance levels are as follows: $^{*}(p < 0.05)$, $^{**}(p < 0.001)$, $^{***}(p < 0.0001)$.

and untrawlable stations for seafloor ruggedness calculated from 3 × 3 and 11 × 11 cell arrays. However, broad-scale ruggedness (VRM 21 × 21 cells) was significantly lower at trawlable stations.

There was a significant difference between oblique incidence S_b and mosaic S_b normalized to oblique incidence angles ($p < 0.0001$), demonstrating that the means of these metrics were different. These metrics were correlated for camera stations ($r = 0.78$).

3.2. Multibeam metrics and haul locations

All angle-dependent S_b metric values for bottom-trawl haul locations classified as trawlable were significantly less than values at untrawlable locations (Fig. 4). These included normal incidence S_b, oblique incidence S_b, and S_b slope near normal incidence. Mosaic S_b values at trawlable haul locations were also significantly lower than untrawlable haul locations.

Only benthic terrain metrics that could discriminate between trawlable and untrawlable camera stations were evaluated in the analysis for haul locations, including VRM and BPI at one derived spatial scale. Although these metrics were discriminatory at camera stations, which sampled a broader range of seafloor types than the BT haul locations, they did not discriminate between trawlable and untrawlable haul locations (Fig. 4).

There was a significant difference between oblique incidence S_b and mosaic S_b normalized to oblique incidence angles ($p < 0.0001$), demonstrating that the means of these metrics were different. These metrics were correlated for haul locations ($r = 0.95$).

3.3. Trawlability models

The most discriminatory single metric models for camera stations based on AIC values were mosaic S_b (AIC = 37.2, $D^2 = 0.38$) and oblique incidence S_b (AIC = 42.5, $D^2 = 0.28$). The best models for camera stations with more than one predictor were models that included broad-scale bathymetric position index (BPI 200 cells) and seafloor ruggedness (VRM 21 cells) with oblique incidence S_b (AIC =

Table 2
Comparison of results from GLM models to predict seafloor trawlability at camera stations. Models are listed by decreasing accuracy of the GLM predictions, expressed by the Akaike Information Criterion (AIC), the proportion of total deviance explained (D^2), and an analysis of deviance test comparing the model results to a null model ($\alpha = 0.05$). Predictor variables are the multibeam-derived seafloor metrics. Angle-dependent backscatter metrics are normal incidence S_b, oblique incidence S_b, and S_b-slope. Mosaic S_b was derived from backscatter mosaics (6 m^2). Benthic terrain metrics derived from bathymetry grids (6 m^2) are seafloor slope, profile curvature, and plan curvature (3 × 3 cell arrays). Seafloor ruggedness (VRM) is calculated from 3 × 3, 11 × 11, and 21 × 21 cells arrays, and bathymetric position index (BPI) is calculated from analysis windows of 20, 50, 100, and 200 cell radius.

Model	AIC	D^2	Model significance
Oblique incidence S_b + BPI_{200} + VRM_{21}	32.1	0.55	***
Mosaic Sb + BPI_{200} + VRM_{21}	32.5	0.54	***
Mosaic Sb + BPI_{200}	35.8	0.44	***
Mosaic Sb + VRM_{21}	37.2	0.42	***
Mosaic Sb	37.2	0.38	***
Oblique incidence S_b + VRM_{21}	38.5	0.39	***
Oblique incidence S_b + BPI_{200}	40.8	0.35	***
Oblique incidence S_b	42.5	0.28	***
VRM_{21}	48.9	0.16	*
VRM_{11}	51.1	0.12	*
BPI_{200}	51.1	0.12	*
BPI_{100}	52.2	0.10	*
VRM_3	53.2	0.08	*
Normal incidence S_b	54.3	0.06	NS
S_b-slope	55.4	0.04	NS
Profile curvature	55.9	0.03	NS
Plan curvature	56.6	0.02	NS
Slope	57.1	<0.01	NS

Significance levels for analysis of deviance tests are as follows: NS (not significant).
* ($p < 0.05$).
** ($p < 0.001$).
*** ($p < 0.0001$).

32.1, $D^2 = 0.55$) or mosaic S_b (AIC = 32.5, $D^2 = 0.54$). The AIC difference for these two models was 0.4 digits, which suggests empirical support for both models. Significant models for camera stations explained a proportion of the total deviance (D^2) that ranged from 0.08 to 0.55 (Table 2).

The most discriminatory single metric model for haul locations was with oblique incidence S_b (AIC = 261.0, $D^2 = 0.24$). A two-metric model that combined oblique incidence S_b and normal incidence S_b was not an improvement as these models are not empirically different (AIC = 260.0, $D^2 = 0.25$). Significant models for haul locations explained a proportion of the total deviance (D^2) that ranged from 0.04 to 0.25 (Table 3).

The models developed using MBES data collected at camera stations that included either oblique incidence S_b or mosaic S_b with broad-scale BPI and VRM were the most discriminatory over all models tested. A probability map of predicted seafloor trawlability for the MBES survey area was generated using the model that included mosaic S_b. This model was $0.36 + [-2.1 * \text{Mosaic } S_b] + [-3.8 * BPI_{200}] + [-1.6 * VRM_{21}]$. This model was selected because the spatial coverage of the map using mosaic S_b would be greater than the model that included the angle-dependent metric oblique incidence S_b.

Probability maps produced using the best-fitting model predicted that trawlable seafloor occurred over 3445 km^2 and untrawlable seafloor accounted for 2544 km^2 (Fig. 5). These maps demonstrated variability in the predicted seafloor trawlability across the GOA, including the fine-scale MBES survey locations with camera stations (Fig. 6) and the BT survey haul locations (Fig. 7). The model developed at camera stations was cross-validated at bottom-trawl haul locations and correctly predicted 69% of sampled trawlable and untrawlable haul locations. For the haul locations, a total of 68% of successful haul locations were correctly assigned as trawlable by the model and 83% of marginal and 73% of failed haul locations were correctly assigned as untrawlable by the model. Trawlable haul locations

Table 3
Comparison of results from GLM models to predict seafloor trawlability at haul locations. Models are listed by decreasing accuracy of the GLM predictions, expressed by the Akaike Information Criterion (AIC), the proportion of total deviance explained (D^2), and an analysis of deviance test comparing the model results to a null model ($\alpha = 0.05$). Predictor variables are the multibeam-derived seafloor metrics. Angle-dependent backscatter metrics are normal incidence S_b, oblique incidence S_b, and S_b-slope. Mosaic S_b was derived from backscatter mosaics (6 m^2). Benthic terrain metrics derived from bathymetry grids (6 m^2) are VRM 21 × 21 cells and BPI 200 cells.

Model	AIC	D^2	Model significance
Oblique incidence S_b + normal incidence S_b	260.0	0.25	***
Oblique incidence S_b	261.0	0.24	***
Mosaic S_b + normal incidence S_b	274.7	0.21	***
Mosaic S_b	278.0	0.19	***
Normal incidence S_b	304.5	0.11	***
S_b-slope	340.1	0.04	**
VRM_{21}	342.4	<0.01	NS
BPI_{200}	342.4	<0.01	NS

Significance levels for analysis of deviance tests are as follows: NS (not significant).
* ($p < 0.05$).
** ($p < 0.001$).
*** ($p < 0.0001$).

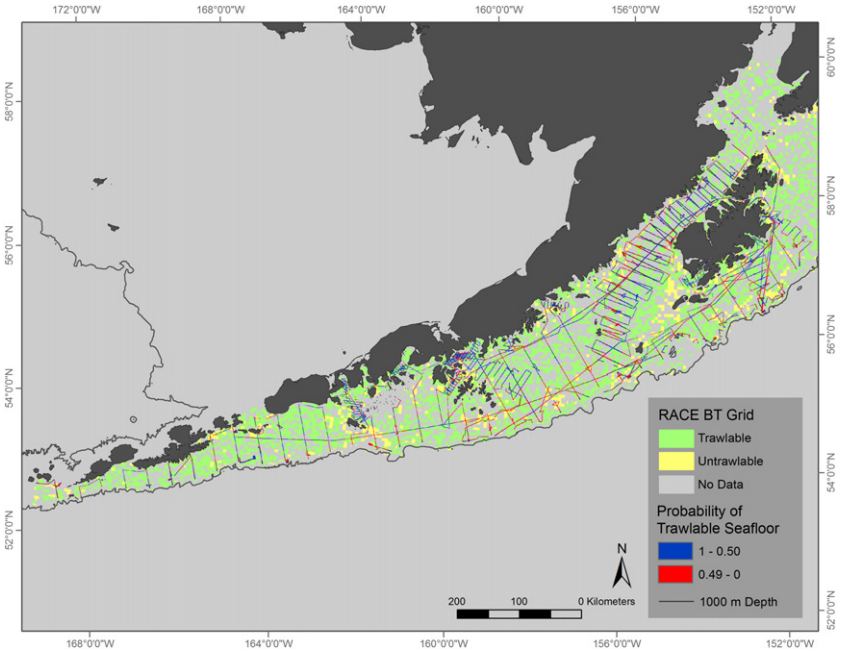

Fig. 5. Probability of trawlable seafloor for the ME70 MBES survey footprint in the GOA. The probability surface is derived from the following logistic regression model created from data at camera stations: $0.36+[-2.1*\text{Mosaic}S_b]+[-3.8*BPI_{200}]+[-1.6*VRM_{21}]$. Areas of the seafloor with high probability of being trawlable are blue and areas with low probability of being trawlable (i.e., untrawlable) are red, classified based on a model threshold value of 0.5 from a probability scale of 1–0 for trawlable and untrawlable seafloor. The RACE BT survey sampling grid shows qualitatively classified trawlable grid cells (green), qualitatively classified untrawlable cells (yellow), and cells that are not designated as trawlable or untrawlable (gray). (For interpretation of the references to colour in this figure legend, the reader is referred to the web version of this article.)

(successful hauls) had a 62% ± 29% (mean ± SD) probability of being trawlable and untrawlable haul locations (marginal and failed hauls) had a 38% ± 22% probability of being trawlable.

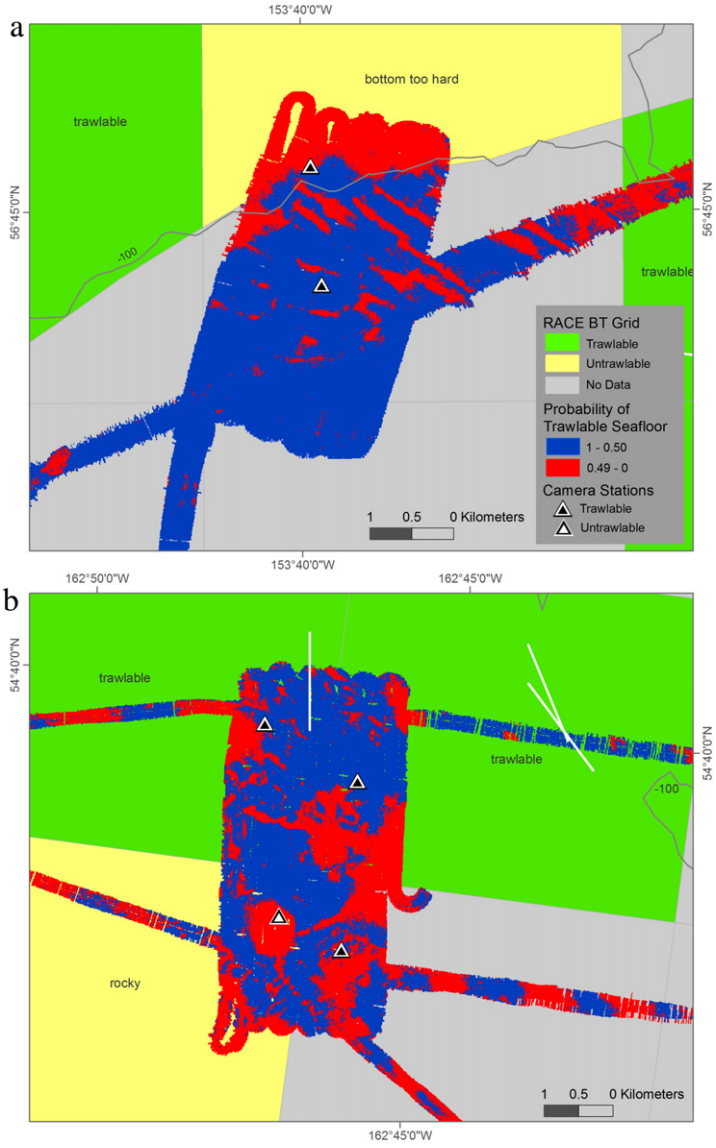

Fig. 6. Probability of trawlable seafloor at ME70 MBES fine-scale survey locations (a, b), with camera stations in the RACE BT survey area. Areas of the seafloor with high probability of being trawlable are blue and areas with low probability of being trawlable (i.e., untrawlable) are red. The survey locations intersect the BT survey sampling grid, including several qualitatively classified trawlable grid cells (green), qualitatively classified untrawlable cells (yellow), and cells that are not designated as trawlable or untrawlable (gray). Three successful bottom-trawl haul locations (white lines) intersect areas of trawlable seafloor predicted by the model (b). (For interpretation of the references to colour in this figure legend, the reader is referred to the web version of this article.)

4. Discussion

Angle-dependent S_b distinguished between trawlable and untrawlable seafloor types across incidence angles at camera stations and haul locations. Trawlable locations had lower S_b values overall, which likely corresponded to sediments of finer grain size or the lack of strong scatterers such as boulders and rock (Jackson and Richardson, 2007). Oblique incidence S_b was the most discriminatory

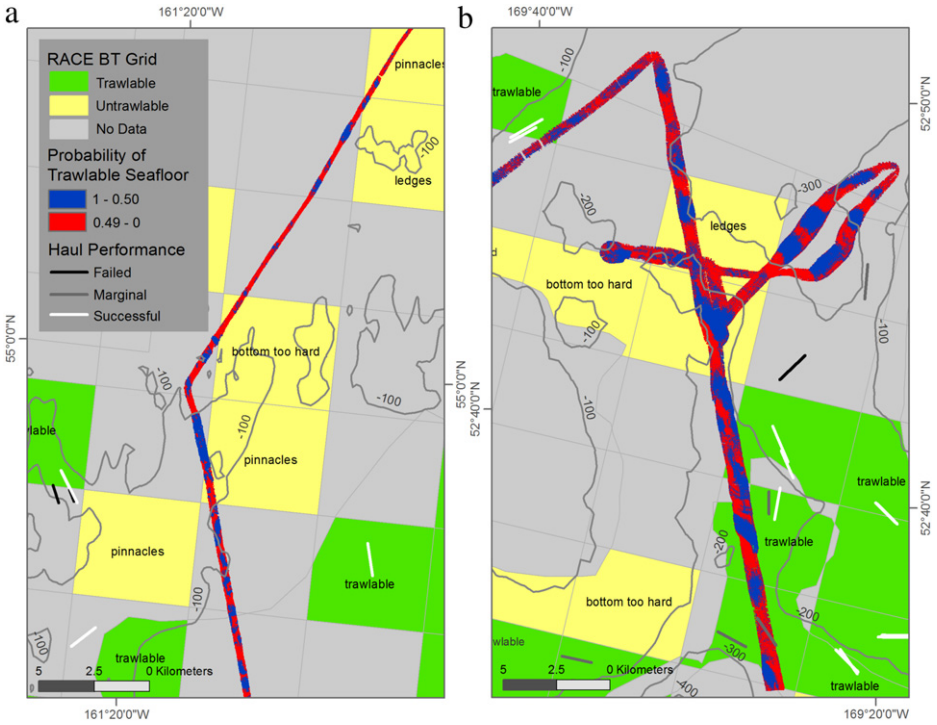

Fig. 7. Probability of trawlable seafloor for sections of the ME70 MBES survey trackline in the RACE BT survey area (a, b). Areas of the seafloor with high probability of being trawlable are blue and areas with low probability of being trawlable (i.e., untrawlable) are red. The multibeam survey trackline intersects the BT survey sampling grid, including several previously qualitatively classified trawlable grid cells (green) and untrawlable cells (yellow), as well as cells that are not designated as trawlable or untrawlable (gray). Haul locations, including successful (white), and marginal (dark gray) and failed (black) due to gear damage, are interspersed throughout these areas. (For interpretation of the references to colour in this figure legend, the reader is referred to the web version of this article.)

single angle-dependent metric for camera stations and haul locations. Normal incidence S_b was only useful in predictive models of seafloor trawlability for haul locations, where it was one of the two best models when combined with oblique incidence S_b. Although normal incidence S_b and S_b-slope were discriminatory for both data sets, sample size may have limited the utility of these other angle-dependent S_b metrics when evaluating camera stations. This is similar to the results of Weber et al. (2013). Nonetheless, our results demonstrate that the seafloor mapping protocol developed by Weber et al. (2013) at Snakehead Bank for the ME70 MBES, using angle-dependent S_b and other multibeam-derived seafloor metrics, can be applied broadly for the GOA.

Mosaic S_b was included in the effort to develop a broad-scale seafloor trawlability model for the GOA. Trawlable and untrawlable locations from both data sets were often detected using mosaic S_b. As a single metric, mosaic S_b was the best predictor for seafloor trawlability using MBES data collected at camera stations and the second best metric after oblique incidence S_b for haul locations. Mosaic S_b is a commonly used backscatter product that has become more widely available outside the hydrographic community to characterize and map seafloor habitat (Anderson et al., 2008; Brown et al., 2011; Buhl-Mortensen et al., 2012).

The nature of mosaic S_b and angle-dependent S_b metrics should be considered when examining the predictive power of these metrics. Backscatter mosaics are generated by normalizing S_b values across the multibeam swath to the range of observed values at oblique incidence angles (Rzhanov et al., 2012). This procedure requires that normal incidence S_b is treated as if it has the same discriminatory power as oblique incidence S_b when this is not strictly true (Figs. 1 and 2). Due to the procedure by which backscatter mosaics are produced, it is likely that mosaic S_b and the S_b metric at oblique

incidence angles are not effectively different metrics with regard to these data sets. These metrics were correlated for both the camera station and haul location data sets. However, these metrics had different discriminatory ability in models of seafloor trawlability, which suggests that they are related, complementary metrics.

Bathymetric position index (BPI) and seafloor ruggedness (VRM) were discriminatory terrain metrics at all spatial scales analyzed for trawlable and untrawlable camera stations. However, seafloor slope and curvature were not helpful in this regard. None of the bathymetry metrics tested for bottom-trawl haul locations were discriminatory. The power of multibeam-derived terrain metrics to predict seafloor features of interest depends on application and spatial scale (Wilson et al., 2007). For example, BPI and terrain aspect, which is the orientation of the steepest gradient of slope, are important in combination to describe habitat for animals like corals that occur on emergent seafloor features and orient with current direction for feeding (Dolan et al., 2008). In contrast, BPI was important for predicting seafloor trawlability, but aspect would not likely matter.

Backscatter metrics alone were better predictors of seafloor trawlability than BPI and VRM derived from gridded bathymetry data. Backscatter values that correspond to locations of untrawlable seafloor types are still only a proxy for a variety of features that could snag bottom-trawl gear. Depending on the application, it is tempting to argue that certain seafloor terrain metrics indicate the presence of rock or rocky features when these metrics represent proxies for seafloor types that could be rock. This may be a particular temptation when backscatter data or other direct measures of surficial substrate qualities are not available and terrain metrics derived from bathymetry data are relied upon. In the case of bottom-trawl haul locations, optical groundtruth data collected at appropriate spatial scales should help to identify the nature of untrawlable features predicted to occur in the MBES survey area.

A potential limitation in using seafloor terrain metrics with MBES survey trackline data is that the spatial scale of the neighborhoods required to calculate these metrics is limited by the multibeam swath width. This will become a larger issue when calculating these metrics at broader-spatial scales, when the metric will only be computed for sections of the swath where the entire analysis window is fulfilled. This is not likely a limitation for MBES data collected from areas with 100% bottom coverage, such as the fine-scale survey locations sampled in 2011.

Camera stations and bottom-trawl survey haul locations produced different broad-scale seafloor trawlability models for the GOA. Backscatter metrics were useful to distinguish between trawlable and untrawlable conditions with both data sets. However, seafloor terrain metrics derived from bathymetry data were useful only to distinguish between conditions for camera stations. This is because the camera stations likely represented a broader range of seafloor types encountered by the MBES survey than the haul locations, which had been preselected as locations that were likely trawlable during groundfish BT survey operations. This was apparent, for example, when examining the differences between the mean and the spread of the values for broad-scale BPI and VRM calculated for each data set (Figs. 3 and 4).

The results indicated that the camera data produced better models predicting seafloor trawlability than the BT survey data. This is likely caused by the scale and characteristics of the data collected for each of the models. For the bottom-trawl haul path model, the MBES metrics were integrated over bottom-trawl tows that were conducted over multiple hectares, on, at worst, marginally trawlable seafloor. In contrast, the camera drops were collected over hundreds of meters and over a much greater variety of seafloor types in the study area. The camera data therefore provided much more contrast in conditions (trawlable seafloor, marginally trawlable and untrawlable seafloor) and a much better spatial resolution to those conditions. The definition of untrawlable seafloor used when characterizing video data collected at camera stations (i.e., having a 25 cm or larger boulder or rock present), although a relatively arbitrary decision that was based on the trawl footrope characteristics, appeared to reasonably capture the difference between trawlable and untrawlable seafloor in the BT survey area, as evidenced by the model fit.

The two best models of seafloor trawlability for the GOA survey area included either oblique incidence S_b or mosaic S_b with BPI and VRM derived at broad-spatial scales developed from MBES data sampled at camera stations. These models were most discriminatory over all models tested and were not different in their relative discriminatory power. Because oblique incidence S_b is an angle-dependent metric, maps of predicted seafloor trawlability using this metric were limited in spatial

coverage compared to maps using the model with mosaic S_b. The mosaic S_b model produced a map with the greatest spatial coverage, which may be more useful in practice.

This broad-scale GOA seafloor trawlability model and map have the potential to improve how the BT survey identifies trawlable and untrawlable locations. The trawlability map crosses several areas of the BT survey sampling grid that are not classified as trawlable or untrawlable (Fig. 5). The model map can help inform a trawlability classification for these survey grid cells. The model can also be used to extend a quantitative classification to areas that are currently qualitatively classified as trawlable or untrawlable by the BT survey researchers. For example, untrawlable areas near the slope include several grid cells with the qualitative designation as untrawlable (Fig. 5). The extent of these areas could be updated using the model result with a specified threshold and then surveyed more extensively using the ME70 MBES with optical groundtruth sampling to identify specific features of interest.

The concept of spatial scale is an important consideration with respect to using the model map. Much more fine-scale variation is detected from the map produced using MBES data gridded to 6 m^2 resolution than would be detected if the model results were mapped at a coarser resolution, such as the 5 km^2 sampling grid used by the BT survey for groundfish (Figs. 6 and 7). A finer-scale trawlability classification for the GOA presents an opportunity to identify untrawlable features that are not known for the current BT survey sampling grid or even visible on current navigational charts (Table S1; see Appendix A). This may assist BT survey personnel to avoid certain untrawlable features, which may otherwise be missed using only single-beam echosounders to search for trawlable ground. This has great potential to help optimize BT survey operations in sampling groundfish populations in areas, which are likely trawlable.

A model and map of predicted seafloor trawlability across the greater GOA applies more broadly than optimizing BT survey efficiency and avoiding gear damage. This information will help describe the distribution of commercially harvested groundfish species that occur in either trawlable, untrawlable, or mixed habitats. For example, many harvested rockfishes associate with rugged and rocky untrawlable habitat where it is difficult to obtain biomass estimates using traditional BT survey methods. Instead, biomass estimates for these species are extrapolated to untrawlable areas from trawlable sample locations where they are captured by the BT survey. Biomass for rockfishes in untrawlable habitat on Snakehead Bank, sampled using a combined acoustic-camera survey, was estimated to be 5–60 times greater than the biomass estimated for these species using traditional bottom-trawl sampling gear (Jones et al., 2012). In contrast, biomass estimates for flatfish in trawlable areas sampled using an occupied submersible were 10 times higher in these habitats than in surrounding untrawlable locations (Jagielo et al., 2003). The GOA-wide trawlability model and map that includes both multibeam backscatter and bathymetry metrics has the potential to be an indispensable resource to develop habitat-specific assessments to improve biomass estimates for numerous groundfish species.

Acknowledgments

The authors would like to thank the captains and crews of the NOAA ship *Oscar Dyson* and the following individuals for their assistance with this project: J. Beaudoin, B. Calder, M. Doucet, S. Furnish, J. Heifetz, D. Jones, S. Kotwicki, L. Mayer, A. McCarthy, P. Ressler, G. Rice, S. Stienessen, R. Towler, and P. Walline. We also thank the many scientists at the Alaska Fisheries Science Center who collected the bottom trawl survey data. Thank you to J. Heifetz, P. von Szalay, J. Napp, and two anonymous reviewers for their helpful critiques of this manuscript. This project was funded by the Alaska Fisheries Science Center and the University of New Hampshire Center for Coastal and Ocean Mapping/NOAA Joint Hydrographic Center.

The findings and conclusions in the paper are those of the authors and do not necessarily represent the views of the National Marine Fisheries Service. Reference to trade names does not imply endorsement by the National Marine Fisheries Service.

Appendix A. Supplementary data

Supplementary material related to this article can be found online at http://dx.doi.org/10.1016/j.mio.2015.06.001.

References

Anderson, J.T., Van Holliday, D., Kloser, R., Reid, D.G., Simard, Y., 2008. Acoustic seabed classification: current practice and future directions. ICES J. Mar. Sci. 65, 1004–1011.

APL (Applied Physics Laboratory), 1994. High-frequency Ocean Environment Acoustic Models Handbook. University of Washington, Seattle.

Brown, C.J., Smith, S.J., Lawton, P., Anderson, J.T., 2011. Benthic habitat mapping: A review of progress towards improved understanding of the spatial ecology of the seafloor using acoustic techniques. Estaur. Coast. Shelf Sci. 92, 502–520.

Buhl-Mortensen, L., Buhl-Mortensen, P., Dolan, M.F.J., Dannheim, J., Bellec, V., Holte, B., 2012. Habitat complexity and bottom fauna composition at different scales on the continental shelf and slope of northern Norway. Hydrobiologia 685, 191–219.

Buhl-Mortensen, P., Dolan, M., Buhl-Mortensen, L., 2009. Prediction of benthic biotopes on a Norwegian offshore bank using a combination of multivariate analysis and GIS classification. ICES J. Mar. Sci. 66, 2026–2032.

Burnham, K.P., Anderson, D.R., 2002. Model Selection and Multi-Model Inference: A Practical Information-theoretic Approach. Springer, New York, p. 488.

Clausen, D., Heifetz, J., 2002. The northern rockfish, *Sebastes polyspinis*, in Alaska: commercial fishery, distribution, and biology. Mar. Fish. Rev. 64, 1–28.

Cordue, P.L., 2007. A note on non-random error structure in trawl survey abundance indices. ICES J. Mar. Sci. 64, 1333–1337.

Cutter, G.R., Berger, L., Demer, D.A., 2010. A comparison of bathymetry mapped with the Simrad ME70 multibeam echosounder operated in bathymetric and fisheries modes. ICES J. Mar. Sci. 67, 1301–1309.

Dolan, M.F.J., Grehan, A.J., Guinan, J.C., Brown, C., 2008. Modelling the local distribution of cold-water corals in relation to bathymetric variables: Adding spatial context to deep-sea video data. Deep-Sea Research Part I-Oceanographic Research Papers 55, 1564–1579.

Dormann, C.F., Elith, J., Bacher, S., Buchmann, C., Carl, G., Carré, G., Marquéz, J.R.G., et al., 2013. Collinearity: a review of methods to deal with it and a simulation study evaluating their performance. Ecography 36, 027–046.

Duff, A.A., 2008, Using general linear models and ordinary kriging to map species distribution. Appenidx C. Step by step invasive alien plant predictive mapping methods for the Klamath Network, NPS.

Evans, I.S., 1980. An integrated system of terrain analysis and slope mapping. Zeitschrift für Geomorphologic Suppl-Bd 36, 274–295.

Fonseca, L., Brown, C., Calder, B., Mayer, L., Rzhanov, Y., 2009. Angular range analysis of acoustic themes from Stanton Banks Ireland: A link between visual interpretation and multibeam echosounder angular signatures. Appl. Acoust. 70, 1298–1304.

Fonseca, L., Mayer, L., 2007. Remote estimation of surficial seafloor properties through the application Angular Range Analysis to multibeam sonar data. Mar. Geophys. Res. 28, 119–126.

Foote, K.G., Knudsen, H.P., Vestnes, G., MacLennan, D.N., Simmonds, E.J., 1987. Calibration of acoustic instruments for fish density estimation: A practical guide. ICES Cooperative Research Report 144, 69.

Guisan, A., Weiss, S., Weiss, A., 1999. GLM versus CCA spatial modeling of plant species distribution. Plant Ecology 143, 107–122.

Hasan, R.C., Ierodiaconou, D., Laurenson, L., 2012. Combining angular response classification and backscatter imagery segmentation for benthic biological habitat mapping. Estuar. Coast. Shelf Sci. 97, 1–9.

Horn, B.K.P., 1981. Hill shading and the reflectance map. Proc. IEEE 69, 14–47.

Jackson, D.R., Richardson, M.D., 2007. High-frequency Seafloor Acoustics. Springer, New York, p. 338.

Jagielo, T., Hoffmann, A., Tagart, J., Zimmermann, M., 2003. Demersal groundfish densities in trawlable and untrawlable habitats off Washington: implications for the estimation of habitat bias in trawl surveys. Fish. Bull. 101, 545–565.

Jenness, J., 2013, DEM Surface Tools for ArcGIS. Jenness Enterprises.
Available at: http://www.jennessent.com/arcgis/surface_area.htm.

Jones, D., Guttormsen, M., 2012, Results of the acoustic-trawl surveys of walleye pollock (*Theragra chalcogramma*) in the Gulf of Alaska, February–March 2012 (DY2012-01 and DY2012-03). AFSC Processed Rep. 2012–09. 62 pp.

Jones, D.T., Stienessen, S.C., Simonsen, K.A., Guttormsen, M.A., 2015, Results of the acoustic-trawl survey of walleye pollock (*Gadus chalcogrammus*) in the Western/Central Gulf of Alaska, June–August 2011 (DY2011–03). AFSC Processed Rep. 2015–04, 74 p.

Jones, D.T., Wilson, C.D., De Robertis, A., Rooper, C.N., Weber, T.C., Butler, J.L., 2012. Evaluation of rockfish abundance in untrawlable habitat: combining acoustic and complementary sampling tools. Fish. Bull. 110, 332–343.

McCullagh, P., Nelder, J.A., 1983. Generalized Linear Models. Chapman and Hall, London, New York, p. 261.

R Development Core Team, 2013, R: A language and environment for statistical computing. R Foundation for Statistical Computing, Vienna, Austria. ISBN 3-900051-07-0. Available at: http://www.R-project.org.

Reynolds, J.R., Rooney, S.C., Heifetz, J., Greene, H.G., Norcross, B.L., Shotwell, S.K., 2012. Habitats and demersal fish communities in the vicinity of Albatross Bank, Gulf Of Alaska. In: Harris, P.T., Baker, E.K. (Eds.), Seafloor Geomorphology As Benthic Habitat. Elsevier, London, pp. 539–553.

Rooper, C.N., Boldt, J.L., Zimmermann, M., 2007. An assessment of juvenile Pacific Ocean perch (*Sebastes alutus*) habitat use in a deepwater nursery. Estuar. Coast. Shelf Sci. 75, 371–380.

Rzhanov, Y., Fonseca, L., Mayer, L., 2012. Construction of seafloor thematic maps from multibeam acoustic backscatter angular response data. Comput. Geosci. 41, 181–187.

Sappington, J.M., Longshore, K.M., Thompson, D.B., 2007. Quantifying landscape ruggedness for animal habitat analysis: A case study using bighorn sheep in the Mojave Desert. J. Wildl. Manage. 71, 1419–1426.

Schmidt, J., Evans, I.S., Brinkmann, J., 2003. Comparison of polynomial models for land surface curvature calculation. Int. J. Geogr. Inf. Sci. 17, 797–814.

Shotwell, S.K., Heifetz, J., Courtney, D.L., Greene, H.G., 2008. Mapping marine benthic habitat in the Gulf of Alaska: Geological habitat, fish distributions, and fishing intensity. In: Todd, B.J., Greene, H.G. (Eds.), Mapping the Seafloor for Habitat Characterization. Geological Association of Canada, St. John's, Newfoundland, pp. 349–368. Special Paper 47.

Stauffer, G.D., (compiler), 2004, NOAA Protocols for Groundfish Bottom Trawl Surveys of the Nation's Fishery Resources. U. S. Dep. Commerce, NOAA Tech. Memo. NMFS-F/SPO-65, 205 pp.

Stein, D.L., Tissot, B.N., Hixon, M.A., Barss, W., 1992. Fish-habitat associations on a deep reef at the edge of the Oregon continental-shelf. Fish. Bull. 90, 540–551.

Todd, B.J., Kostylev, V.E., 2011. Surficial geology and benthic habitat of the German Bank seabed, Scotian Shelf, Canada. Cont. Shelf Res. 31, S54–S68.
Trenkel, V.M., Mazauric, V., Berger, L., 2008. The new fisheries multibeam echosounder ME70: description and expected contribution to fisheries research. ICES J. Mar. Sci. 65, 645–655.
Von Szalay, P.G., Raring, N.W., Shaw, F.R., Wilkins, M.E., Martin, M.H., 2010, Data Report: 2009 Gulf of Alaska bottom trawl survey. NOAA Tech. Memo. NMFS-AFSC-208. 245 pp.
Weber, T.C., Rooper, C., Butler, J., Jones, D., Wilson, C., 2013. Seabed classification for trawlability determined with a multibeam echo sounder on Snakehead Bank in the Gulf of Alaska. Fish. Bull. 111, 68–77.
Weiss, A., 2001. Topographic position and landforms analysis. In: Poster Presentation. ESRI User Conference, San Diego, CA.
Wentworth, C.K., 1922. A scale of grade and class terms for clastic sediments. J. Geology 30, 377–392.
Williams, K., Rooper, C.N., Towler, R., 2010. Use of stereo camera systems for assessment of rockfish abundance in untrawlable areas and for recording pollock behavior during midwater trawls. Fish. Bull. 108, 352–362.
Wilson, M.F.J., O'Connell, B., Brown, C., Guinan, J.C., Grehan, A.J., 2007. Multiscale terrain analysis of multibeam bathymetry data for habitat mapping on the continental slope. Marine Geodesy 30, 3–35.
Wright, D.J., Pendleton, M., Boulware, J., Walbridge, S., Gerlt, B., Eslinger, D., et al. 2012, ArcGIS Benthic Terrain Modeler (BTM), v. 3.0, Environmental Systems Research Institute, NOAA Coastal Services Center, Massachusetts Office of Coastal Zone Management. Available at: http://esriurl.com/5754.
Zimmermann, M., 2003. Calculation of untrawlable areas within the boundaries of a bottom trawl survey. Can. J. Fish. Aquat. Sci. 60, 657–669.